Photonics-based Multiband Radar Fusion with Millimeter-level Range Resolution

Xin Zhu, Guanqun Sun, and Fangzheng Zhang*
College of Electronic and Information Engineering, Nanjing University of Aeronautics and Astronautics, Nanjing 210016, China
**Email: zhangfangzheng@nuaa.edu.cn*

Abstract: Photonics-based multiband radar fusion is demonstrated in which three photonics-based radars with a 2-GHz bandwidth are successfully fused to have an 18-GHz bandwidth response. Based on this technique, millimeter-level range resolution radar imaging is achieved.

1. Introduction

Microwave photonic technologies have been applied to overcome the bandwidth limitations of traditional radars [1-6]. Thanks to the large operation bandwidth, previously reported photonics-based radars can achieve a high range resolution in the centimeter level [7]. However, due to unavailability of suitable wideband radio frequency (RF) front-ends and strict regulation of the frequency usage in the electromagnetic spectrum, practical applications of photonics-based broadband radars are still challenging. Multiband radar fusion provides a promising solution to this problem, which improves the range resolution by fusing the target frequency responses of different frequency bands of multiple radars into a wider bandwidth frequency response [8]. With this technique, it is possible to achieve a high range resolution using multiple discontinuous spectra and relax the requirements for broadband hardware.

In this report, we demonstrate high-range-resolution target detection and imaging by photonics-based multiband radar fusion. Three photonics-based radars having the same bandwidth of 2-GHz in different frequency ranges are constructed. After multiband fusion, an equivalent 18-GHz operation bandwidth is achieved, enabling a theoretical range resolution as high as ~8.3 mm. In the experiment, two targets having a distance of 9 mm along the radar line of sight are successfully distinguished after multiband fusion. Synthetic aperture radar imaging is also implemented, which further verifies the advantage of the photonics-based multiband radar fusion technique.

2. Principle

The three photonics-based radars work in different frequency ranges of 18-20 GHz, 23-25 GHz, and 28-30 GHz, respectively. They have the same basic structure based on photonic frequency multiplication in the transmitter and photonic frequency mixing in the receiver [9], as shown in Fig. 1. In each photonics-based radar, the light from a laser diode (LD) is modulated by a dual-parallel Mach-Zehnder modulator (DPMZM) that is driven by an intermediate frequency (IF)-linearly frequency modulated (LFM) signal that has a bandwidth of 500 MHz. Specifically, the frequencies of the IF-LFM signals in the three radars are 4.5-5 GHz, 5.75-6.25 GHz and 7-7.5 GHz, respectively. By properly setting the bias voltages, the DPMZM works in the frequency quadrupling mode [9]. The output signal is divided into two branches by an optical coupler (OC), and the signal in the upper branch is sent to a photodetector (PD) for optical-to-electrical conversion. The generated LFM signals covering 18-20 GHz, 23-25 GHz and 28-30 GHz, corresponding to the three radars respectively, are amplified by three power amplifiers (PA) before launched into the air. In each receiver, the radar echoes are amplified by a low noise amplifier (LNA) before applied to drive an MZM to modulate the reference optical signal from the lower branch of the OC. The output signal is sent to another PD to implement photonic frequency mixing, which completes the de-chirp processing [10]. Then, the electrical de-chirped signal is selected out by a low pass filter (LPF) and sampled by an analog-to-digital converter (ADC). The digital samples from the three radar receivers are processed in a digital signal processing (DSP) unit.

Since the three photonics-based radars work independently, coherent processing is first performed in the DSP unit to compensate for the incoherent phases (ICPs) between different frequency bands. This is implemented based on the method in [8, 11]. In this method, the all-pole signal model is adopted, which has the form of

$$M(f_n) = \sum_{k=1}^{P} a_k p_k^{\ n} \tag{1}$$

where n, P and a_k are the sample index, the number of scattering centers and their complex amplitudes, respectively. The poles p_k characterize the relative ranges and frequency decay of the individual scattering centers. By choosing one radar as the reference and establishing the all-pole signal models corresponding to the three de-chirped signals, the ICPs can be estimated and compensated [12]. This way, the three de-chirped signals become mutual-coherent signals. Then, the mutual-coherent de-chirped signals are synthesized in time domain. Based on the obtained digital sequence, the number of scattering centers and the poles are estimated applying the unitary estimation of signal parameters via rotational invariance techniques (U-ESPRIT) and the linear least-squares method. After that, the obtained extended all-pole model is used to interpolate between and extrapolate outside of the three frequency bands [8], obtaining an equivalent wideband frequency response.

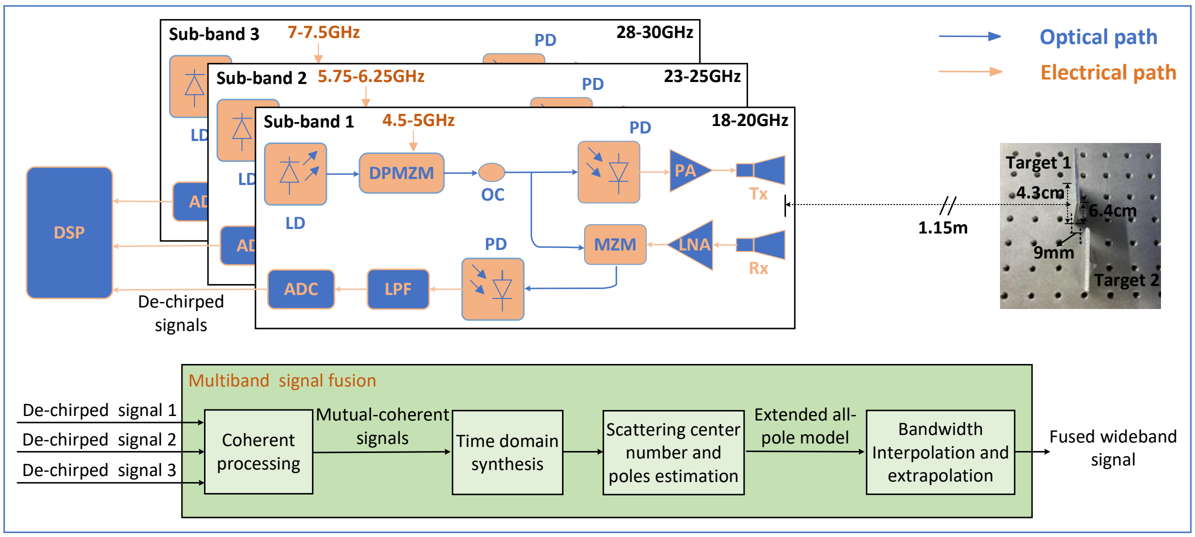

Fig. 1. Setup of the photonics-based radars and the signal processing flow of the multiband fusion.

3. Experiment and results

In the experiment, the targets to be detected are two metallic planes, both having a size of 4.3 cm × 6.4 cm, as shown in Fig. 1. They are placed at about 1.15 m away from the radar antennas and the distance between the two metallic planes is 9 mm along the radar range direction. The de-chirped signals are sampled by a multi-channel real-time oscilloscope (Agilent, DS09404A) with a sampling rate of 200 MSa/s in each channel. The de-chirped signals in a single period are shown in Fig. 2(a), (b) and (c), corresponding to the three photonics-based radars, respectively. The normalized range profiles obtained by performing fast Fourier transformation to the de-chirped signals are shown in Fig. 2(d). Obviously, the two targets cannot be distinguished in the obtained range profiles, which is caused by the fact the distance between the two targets is far less than the range resolution of a 2-GHz bandwidth radar (7.5 cm).

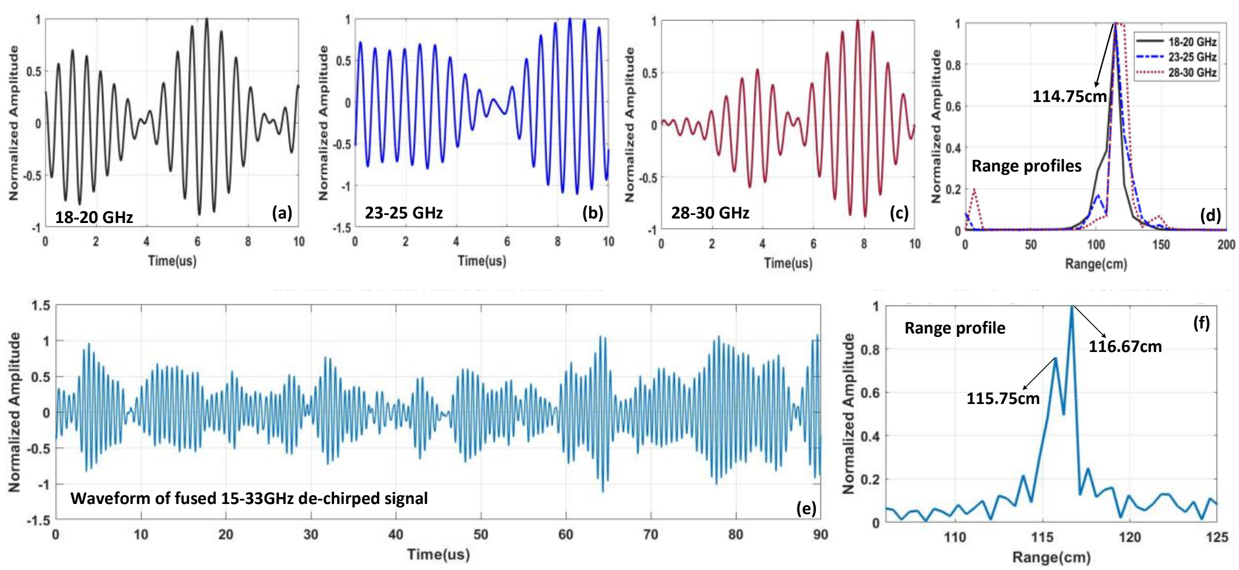

Fig. 2. De-chirped signals of the photonics-based radars working in (a) 18-20 GHz, (b), 23-25 GHz, and (c) 28-30 GHz, respectively, and (d) the corresponding range profiles; (e) the de-chirped signal after multiband fusion to 15-33 GHz, and (f) the corresponding range profile.

By performing multiband fusion according to the method shown in Fig. 1, the de-chirped signal corresponding to a radar with an equivalent bandwidth of 18-GHz (15-33 GHz) is obtained, as shown in Fig. 2(e). The normalized range profile is calculated and shown in Fig. 2(f). As can be seen, the two targets are clearly distinguished and the distance between the two targets is measured to be 9.2 mm, which is very close to the real values. Then, synthetic aperture radar imaging is implemented by moving the antenna pair to form a uniform linear array with 19 equally spaced apertures that have a total length of 34.2 cm, as shown in Fig. 3(a). To satisfy the far field condition and reduce the echo amplitude fluctuations for different apertures, the distance from the targets to the radar array is extended to be about 6.8 m. The radar imaging is implemented by coherent back projection algorithm [13, 14]. Fig. 3(b) shows the imaging result obtained by the single photonics-based radar working in 18-20 GHz. In Fig. 3(b), only one bright spot is observed, indicating the two targets cannot be distinguished in both the range and angular directions. Here, the angular resolution determined by the synthetic radar array is about 1.86°, which is not sufficient to resolve the two targets. After multiband fusion, the constructed image is shown in Fig. 3(c), and the zoom in view around the target area is shown in Fig. 3(d). By comparing these results, it is obvious that the range resolution is greatly enhanced after multiband fusion and the angular resolution remains nearly unchanged. The two targets are easily resolvable in the range direction after multiband fusion.

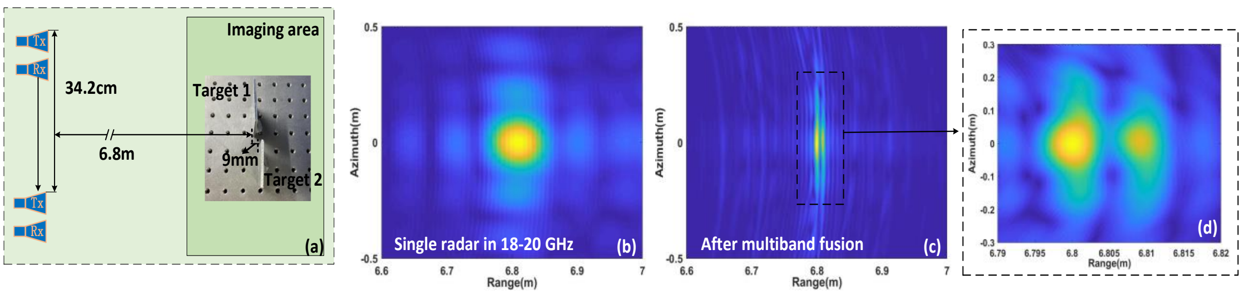

Fig. 3. (a) Illustration of the synthetic aperture array and the targets, (b) the image constructed by a single radar in 18-20 GHz, (c) the image constructed after multiband fusion and (d) the zoom in view around the target area in (c).

4. Conclusion

Photonics-based multiband radar fusion is demonstrated, which is proved to be a good solution for high-range-resolution detection and imaging using discontinuous spectra and hardware with relaxed requirements for bandwidth.

This work was supported by the NSFC program (61871214).

5. References

[1] P. Ghelfi, F. Laghezza, F. Scotti, G. Serafino, S. Pinna, D. Onori, E. Lazzeri, and A. Bogoni, “Photonics in radar systems,” IEEE Microw. Mag, **16**, 74-83 (2015).
[2] J. Yao, “Microwave photonics,” IEEE J Lightwave Technol, **27**, 314–335 (2009).
[3] F. Zhang, Q. Guo, and S. Pan, “Photonics-based real-time ultra-high-range-resolution radar with broadband signal generation and processing,” Sci. Rep., **7**, 13848 (2017).
[4] D. Wu, S. Li, X. Xue, X. Xiao, S. Peng, and X. Zheng, “Photonics based microwave dynamic 3D reconstruction of moving targets,” Opt. Express, **26**, 27659-27667 (2018).
[5] J. Shi, F. Zhang, D. Ben, and S. Pan, “Simultaneous Radar Detection and Frequency Measurement by Broadband Microwave Photonic Processing,” IEEE J Lightwave Technol, **38**, 2171-2179 (2020).
[6] F. Zhang, B. Gao, and S. Pan, “Photonics-based MIMO radar with high-resolution and fast detection capability,” Opt. Express, **26**, 17529-17540 (2018).
[7] Y. Yao, F. Zhang, Y. Zhang, X. Ye, D. Zhu, and S. Pan, “Demonstration of ultra-high-resolution photonics-based Ka-band inverse synthetic aperture radar imaging,” 2018 Optical Fiber Communication Conference (OFC2018), paper. Th3G.5.
[8] K. Cuomo, M., J. E. Piou, and J. T. Mayhan, “Ultra-wideband coherent processing,” IEEE Trans Antennas and Propagation, **47**, 1095–1107 (1999).
[9] B. Gao, F. Zhang, E. Zhao, D. Zhang, and S. Pan, “High-resolution phased array radar imaging by photonics-based broadband digital beamforming,” Opt. Express, **27**, 13194-13203 (2019).
[10] F. Zhang, Q. Guo, Z. Wang, P. Zhou, G. Zhang, J. Sun, and S. Pan, "Photonics-based broadband radar for high-resolution and real-time inverse synthetic aperture imaging," Opt. Express, **25**, 16274-16281 (2017).
[11] D. Xiong, J. Wang, L. Zhao, Z. Yuan, and M. Gao, “Sub-band mutual-coherence compensation in multiband fusion ISAR imaging,” IET Radar Sonar Navig., **13**, 1056–1062 (2019).
[12] B. Tian, Z. Chen, and S. Xu, “Sparse sub-band fusion imaging based on parameter estimation of geometrical theory of diffraction model,” IET Radar Sonar Navig., **8**, 318-326 (2014).
[13] G. Sun, F. Zhang, S. Pan, and X. Ye, “Frequency-domain versus time-domain imaging for photonics-based broadband radar,” Electr Lett, **56**, 1330-1332 (2020).
[14] G. Sun, F. Zhang, B. Gao, Y. Zhou, Y. Xiang and S. Pan, “Photonics-based 3D radar imaging with CNN-assisted fast and noise-resistant image construction,” Opt. Express, **29**, 19352-19361 (2021).